



# Ultra-low-dose intraoperative X-ray imager for minimally invasive surgery: a pilot imaging study

Haewook Park<sup>1,2#</sup>, Kook Nam Han<sup>3#</sup>, Byeong Hyeon Choi<sup>4,5</sup>, Hyunsuk Yoon<sup>1</sup>, Hyun Joon An<sup>1</sup>, Jae Sung Lee<sup>1,2</sup>, Hyun Koo Kim<sup>4,6</sup>

<sup>1</sup>Department of Biomedical Sciences, Seoul National University College of Medicine, Seoul, Republic of Korea; <sup>2</sup>Department of Nuclear Medicine, Seoul National University College of Medicine, Seoul, Republic of Korea; <sup>3</sup>Department of Thoracic and Cardiovascular Surgery, Andong Hospital, Andong, Republic of Korea; <sup>4</sup>Department of Thoracic and Cardiovascular Surgery, Korea University Guro Hospital, Seoul, Republic of Korea; <sup>5</sup>Korean Artificial Organ Center, Korea University, Seoul, Republic of Korea; <sup>6</sup>Department of Biomedical Sciences, Korea University College of Medicine, Seoul, Republic of Korea

**Contributions:** (I) Conception and design: H Park, KN Han, H Yoon, HJ An, HK Kim, JS Lee; (II) Administrative support: HK Kim, JS Lee; (III) Provision of study materials or patients: KN Han, HK Kim; (IV) Collection and assembly of data: H Park, BH Choi; (V) Data analysis and interpretation: H Park, KN Han, HK Kim, JS Lee; (VI) Manuscript writing: All authors; (VII) Final approval of the manuscript: All authors.

<sup>#</sup>These authors contributed equally to this work.

**Correspondence to:** Hyun Koo Kim, MD, PhD. Department of Thoracic and Cardiovascular Surgery, Korea University Guro Hospital, 148, Gurodong-ro, Guro-gu, Seoul 08308, Republic of Korea. Email: kimhyunkoo@korea.ac.kr; Jae Sung Lee, PhD. Department of Nuclear Medicine, Seoul National University College of Medicine, Seoul 03080, Republic of Korea. Email: jaes@snu.ac.kr.

**Background:** With advances in surgical technology, thoracic surgeons have widely adopted minimally invasive limited-resection techniques to preserve normal tissues. However, it remains difficult to achieve *in situ* localization of invisible pulmonary nodules during surgery. Therefore, we proposed an *in situ* ultra-low-dose X-ray imaging device for intraoperative pulmonary nodule localization during minimally invasive surgeries.

**Methods:** The proposed device features a hand-held type and consists of a carbon nanotube-based X-ray source and an intraoral dental sensor. In a preclinical study, we created pseudo pulmonary nodules using *ex vivo* pig lungs. Subsequently, its clinical feasibility was evaluated using *ex vivo* lung cancer specimens from patients with cancer who had undergone minimally invasive surgery.

**Results:** Using the proposed device, we successfully differentiated normal and abnormal tissues from X-ray images of resected lung specimens. In addition, our proposed device only yielded an average radiation dose of 90.9 nGy for a single acquisition of X-ray images and demonstrated excellent temperature stability under consecutive X-ray irradiations. The radiation exposure of our proposed device ( $0.1 \pm 0.0006$   $\mu$ Sv/h) was significantly lower than that of conventional C-arm fluoroscopy ( $41.5 \pm 51.8$   $\mu$ Sv/h). In both preclinical and clinical studies, the margin of nodule shadows was clearly visualized using the proposed device.

**Conclusions:** The proposed device substantially reduced radiation exposure to staff and patients and may allow *in situ* localization of pulmonary nodules. Our proposed device clearly revealed the margins of lung nodules with radiocontrast injection and showed the potential to identify solid nodules without the use of radiocontrast agents.

**Keywords:** Ultra-low-dose; X-ray imaging; minimally invasive surgery; lung cancer

Submitted Nov 14, 2021. Accepted for publication Feb 28, 2022.

doi: 10.21037/tlcr-21-909

View this article at: <https://dx.doi.org/10.21037/tlcr-21-909>

## Introduction

Lung cancer is the leading cause of cancer-related deaths, and its incidence is increasing worldwide (1). According to epidemiology reports on non-small cell lung cancer (NSCLC), cancer-related deaths mostly occur in people over the age of 65 years (2). With the introduction of lung cancer screening programs with low-dose chest computed tomography (CT) scans, thoracic surgeons frequently encounter incidental findings of lung lesions suspected of malignancy (e.g., solid lesions >8 mm or subsolid lesions  $\geq 6$  mm), which require subsequent percutaneous transthoracic needle biopsy for selected populations (3). However, percutaneous biopsy may not provide findings for semi-solid or pure ground-glass nodules, and surgeons cannot access central or perivascular lesions because of serious fatal complications associated with percutaneous procedures (4,5). Video-assisted thoracoscopic surgery (VATS) may be an alternative option to provide tissue specimens for accurate diagnosis, followed by anatomical lobe resection during surgery (6). If indicated, sublobar resection, including wedge resection or segmentectomy, may also be considered to preserve pulmonary function in selected patients with small (<2 cm) peripheral lung cancers (7). Recent studies have shown that sublobar resection performed with an appropriate localization procedure can yield oncological results similar to those of conventional total lobectomy (8-10). Therefore, there has been growing interest in various localization techniques to visualize the exact location of the lesion or provide adequate resection margins during image-guided surgery (11,12).

Direct finger palpation through a small incision or indirect palpation with a surgical instrument can be used to guide the target lesion during VATS. However, the success rate is relatively low (approximately 30–40%) and often results in subsequent conversion to open thoracotomy. Therefore, various image-guided localization techniques have been proposed, including hook wires (13-16), microcoils (17,18), radiocontrast agents (19-21), radioisotopes (13), and fluorescent dyes (22,23). These techniques are applied before surgery under CT or electromagnetic navigational bronchoscopy guidance (24). Surgeons then use C-arm fluoroscopy (25,26), cone-beam CT (27,28), radioprobe (13) or near-infrared camera (29,30) during surgery to support the exact identification of lung lesions.

However, real-time fluoroscopy and CT scans cause a high risk of radiation hazard to both patients and surgical

teams (31) because the long-term use of heavy radiation-protective garments (32) is associated with the occupational hazard of musculoskeletal pain and fatigue in surgical team members. In addition, fluoroscopic C-arm and CT require additional space in the operating room and personnel to operate them.

To overcome these limitations and improve the localization capability of current techniques used for image-guided surgery, we developed an intraoperative X-ray device. Our proposed device is a hand-held and clamp-shaped endoscopic instrument that employs a carbon nanotube (CNT)-based X-ray source, allowing for a compact design that is optimal for VATS and ultra-low-dose X-ray imaging (*Figure 1*). We present the following article in accordance with the ARRIVE reporting checklist (available at <https://tldr.amegroups.com/article/view/10.21037/tlcr-21-909/rc>).

## Methods

### *Development of intraoperative X-ray imager*

The proposed device is a hand-held X-ray device that employs a compact X-ray source (VSI, Korea) based on CNTs. The maximum tube voltage and current of the X-ray source were 60 kVp and 3 mA, respectively. The X-ray source was 15 mm in diameter and 75 mm in length, covered with a ceramic-based material for low-energy X-ray filtering and leakage shielding (*Figure S1*). Unlike conventional X-ray generators used for CT or C-arm fluoroscopy, our imaging protocol only requires X-ray irradiation for 20 ms; therefore, the X-ray device does not require an additional cooling module. We used a dental X-ray sensor (HDR-600, Handy, China) suitable for low-dose X-ray imaging. The X-ray sensor has a field-of-view (FOV) of 36 mm  $\times$  27 mm and offers high spatial resolution of 12 to 14 line-pair/mm.

To explore the feasibility of proximal X-ray imaging, X-ray images were obtained while changing the distance between the radiation source and sensor in the range of 1–5 cm (*Figure S2*). Proximal X-ray imaging studies have shown that our device requires a sufficient source-to-sensor distance of at least 4 cm to avoid image distortion in terms of the saturation of the X-ray pixel intensity.

The proposed X-ray device is equipped with imaging and tissue clamping modules, as follows (*Figure S3*):

- (I) Imaging module (X-ray source, sensor, and sensor manipulator): both the X-ray source and sensor are covered with thin acetal-based plastic. The X-ray

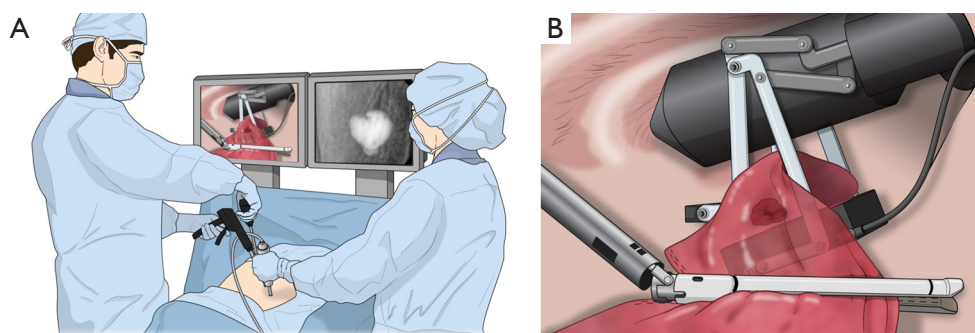


**Figure 1** Minimally invasive thoracoscopic surgery for pulmonary nodules. (A) Intraoperative imaging; (B) resection of pulmonary lesion guided by proposed X-ray device.

source is installed on the top of the insertion body to irradiate the X-rays toward the central FOV of the X-ray sensor installed at the bottom of the insertion body. The X-ray source and sensor are designed to be aligned and spaced from each other at a distance of 4 cm inside the human body to achieve uniform irradiation throughout the sensor FOV.

- (II) Tissue clamping module (clammer and clamp modulator): the tissue clamping module includes a clamper made of aluminum. The clamp is designed to fix the tissue slightly and prevent unwanted movement while intraoperative X-ray imaging is performed. The clamper manipulator allows the position of the clamper to be adjusted such that the clamper can move freely between the X-ray source and the sensor.

Figure S3 shows the step-by-step operation of the device. The X-ray imaging device was designed to be inserted into the human body by moving the sensor manipulator forward to achieve a minimal insertion diameter. Next, the X-ray source and sensor are separated from each other by pulling the sensor manipulator inside the human body. Once the target lesion is well placed by adjusting the clamper manipulator, X-ray images are obtained.

The operation of our device based on the CNT source is digitally manipulated based on a digital function generator and a field-emission transistor-based control module for X-ray emission and parameter adjustment (e.g., tube voltage, tube current, and exposure time). X-ray imaging is performed by triggering the X-ray source using an external footswitch. When switched on, the X-ray is emitted for a pre-set exposure time at a fixed tube voltage and current. The acquired images are then transferred to the data

acquisition computer via the universal serial bus (USB) 2.0 serial communication protocol, and the acquired images are displayed through the monitor and automatically saved to the computer. The total data acquisition time was less than 5 s, including 20 ms of X-ray irradiation. Custom-made data acquisition software provides post-processing of the acquired X-ray images, including image rotation, color map inversion, and brightness and contrast adjustment.

### *System characterization*

The equivalent radiation dose for a single shot scan was measured using a calibrated radiation dosimeter (RaySafe, Sweden). The dosimeter was installed 1 m from the focal spot of the X-ray source. In the measurements, we averaged the radiation dose for 10 consecutive X-ray shots using the following parameters: tube voltage, 40 kVp; tube current, 2 mA; and exposure time, 20 ms.

The spatial resolution of the X-ray imaging system developed in this study was measured using a standard X-ray lead bar phantom (07-553; Fluke Biomedical, US), which featured multiple lead bars of varying sizes ranging from 0.25 to 10 line-pair/mm. The phantom images were acquired using the same X-ray irradiation parameters used in the radiation conduction measurement experiment, mentioned above (i.e., tube voltage of 40 kVp, tube current of 2 mA, and exposure time of 20 ms).

### *Animal models*

Animal experiments were performed under a project license (No. KOREA-2017-0030) granted by institutional review board of Korea University College of Medicine, in compliance with institutional guidelines for the care and use

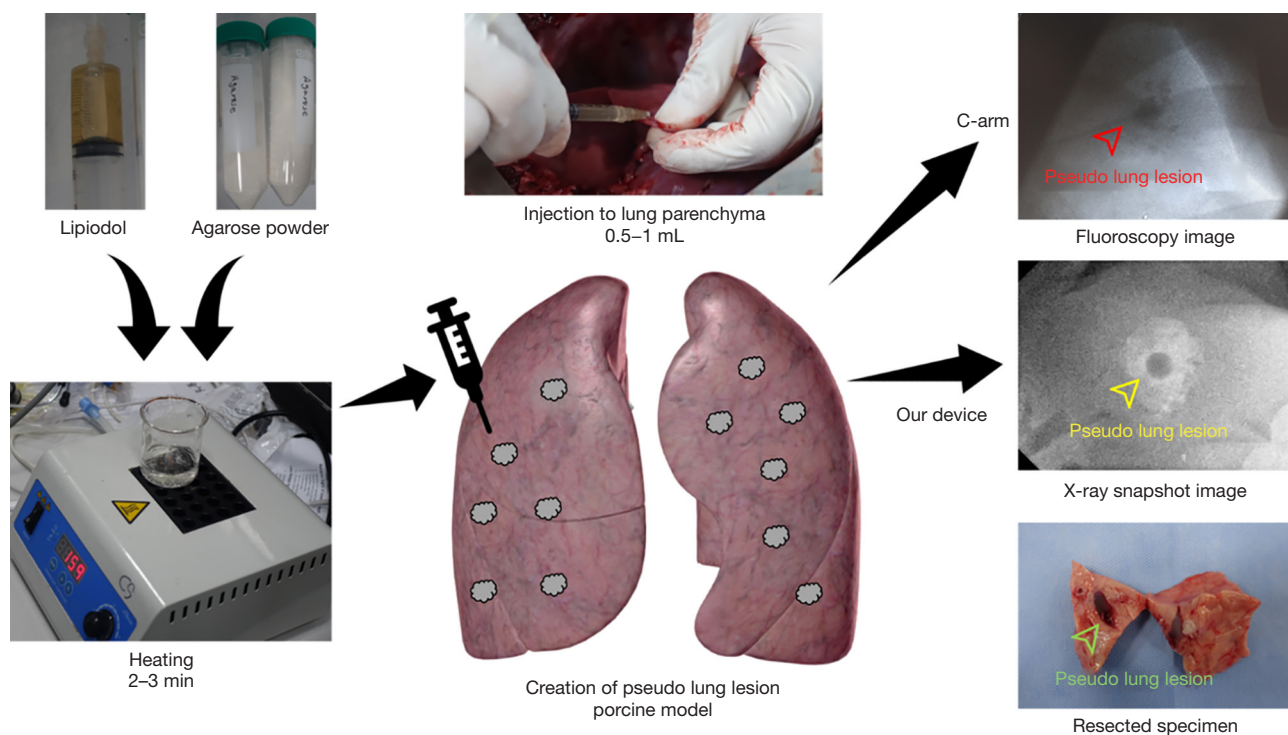


**Figure 2** Creation of pseudo lung lesion using agar and lipiodol in porcine model.

of animals.

In this study, we used a pig *ex vivo* lung to create pseudo lung lesions. Under general anesthesia, the pig was then intubated and ventilated with 50% oxygen at a respiratory rate of 18/min with a tidal volume of 10 mL/kg. Continuous isoflurane inhalation (2–3%) was used to maintain an appropriate level of anesthesia. At the left lateral decubitus position, the entire lung was exposed through a left thoracotomy. Pseudonodules were created by direct injection of 1–2 mL of liquid agar mixed with lipiodol into the lung parenchyma at different locations and depths from the pleura, as shown in *Figure 2*.

The X-ray device was placed on the lung surface, the pseudo lung nodule was grasped, and spot images were obtained using the proposed devices. Various exposure times, voltages, and amplitudes of the X-ray source were tested to derive optimized device settings for lung nodule identification. The lungs were harvested after euthanasia. The lung tissues, including localized pseudo lung lesions, were palpated and bluntly excised. We compared the photographic images of the gross specimen with the radiologic images obtained using the proposed device.

### *VATS in animal model with pseudo lung lesion*

*In vivo* and *ex vivo* X-ray imaging studies were performed using an animal model. Under general anesthesia, a double-lumen endotracheal tube was inserted into the trachea through a tracheostomy while maintaining one-lung ventilation. In the lateral decubitus position, VATS ports were created for the simulation. After the lungs were fully deflated, a mixture of agar and lipiodol heated to 150 °C was injected to create pseudo lung nodules. The insertion body of the proposed device was placed on the lung surface, and the lung tissue was grasped to examine the nodule. After locating the target, the parenchyma was grasped with clamping jaws, and the nodule was excised with an endoscopic stapler. Finally, we examined the resected lung to identify the lesions and corresponding radiographic images (*Figure S4*).

### *Lesion detectability assessment*

We assessed lesion detectability depending on the concentration of the radiocontrast agent and depth of the pseudonodules (*Figure S5*). Pseudonodules were created using heated agar and lipiodol in the whole pig lung. The

**Table 1** Groups by the injection dose and depth from the pleura

Group number	Injection dose (mL)	Injection depth from pleural surface (mm)
1	1	5
2	2	5
3	1	10
4	2	10

four pseudonodules were grouped according to the amount of agar and Lipiodol mixture and the depth from the visceral pleura in the deflated pig lung (*Table 1*).

In group 4, we failed to detect two pseudolesions because the agar with lipiodol was extravasated. We evaluated the lesion detectability of our device in terms of signal-to-noise ratio (SNR) as follows:

$$SNR = 10 \cdot \log \left( \frac{\mu_{nodule}}{\sigma_{background}} \right) dB \quad [1]$$

where  $\mu_{nodule}$  is the mean pixel intensity drawn around pseudo lung nodules and  $\sigma_{background}$  is the standard deviation of pixel values, measured at the image background.

In addition, we preliminarily evaluated the X-ray image quality of 17 lung nodule samples obtained from patients with cancer. Five samples were imaged using radioactive agents and 12 were imaged without injecting a radioactive agent. X-ray imaging of human cancer specimens was performed *ex vivo* using the proposed device. The study was conducted in accordance with the Declaration of Helsinki (as revised in 2013) and approved by institutional board of Korea University Guro Hospital (No. 2017GR0018). Informed consent has been obtained from all individual participants included in this study.

## Results

### System characteristics

When measured using a radiation dosimeter placed 1 m in front of the X-ray focal spot, the radiation dose was  $129 \pm 16$  nGy/shot. The radiation dose was  $53 \pm 10$  nGy/shot when the dosimeter was placed behind the X-ray focal spot (*Figure S6*). In addition, our proposed device clearly resolved the lead bar patterns with a spatial resolution of up to 8.5 line-pair/mm, which was sufficient to determine the resection margin of lung nodules through the X-ray images obtained using the proposed device.

### *In vivo and ex vivo detection of pseudonodules*

X-ray images of the pig models captured with the proposed device are shown in *Figure 3*. The pseudonodules, created in the lung parenchyma by injecting a mixture of agar and lipiodol, also known as ethiodized oil, are indicated by arrows. In the pig models, *in vivo* X-ray images were captured and *ex vivo* X-ray images were captured after lung resection. *Figure S7* shows the *ex vivo* X-ray images obtained using the proposed device and the corresponding CT images (Brilliance 64; Philips, Amsterdam, Netherlands) of pseudonodules in pigs created with different volumes of the agar and lipiodol mixture (1 and 2 mL) and at different pleural depths (0.5 and 1 cm). Four nodules in groups 1, 2, and 3 and two nodules in group 4 were detected on our device. The SNR values of the detected pseudolesions in the X-ray images are summarized in *Table S1*.

The borders of the nodular shadows are clearly shown in the X-ray images taken by our proposed device, except for the images in *Figure S7*, in which the radiocontrast has been extravasated. No image quality degradation was observed owing to the change in the pleural depth of the nodule.

During the simulation in pigs, the radiation exposure rate of the proposed device was measured using a radiation dosimeter (PM1405, POLIMASTER, Belarus) and compared with that of the conventional C-arm (C-arm Ziehm Vision, Ziehm Imaging GmbH, Nuremberg, Germany) and mini C-arm devices (Star-X Intraoral X-ray, HDX Will, Seoul, Republic of Korea). As shown in *Figure S8*, the proposed device ( $0.1 \pm 0.0006$   $\mu$ Sv/h) yielded significantly lower radiation than conventional C-arm fluoroscopy ( $41.5 \pm 51.8$   $\mu$ Sv/h) and mini C-arm for dental or hand surgery ( $6.9 \pm 5.4$   $\mu$ Sv/h). In addition, no change in temperature was observed when measuring the temperature of the plastic cover of the clamp body after 12 consecutive irradiations every 5 s, which addressed the potential safety issue owing to thermal damage to normal tissues (*Figure S9*).

### *Ex vivo imaging of human lung cancer specimens*

To evaluate the clinical applicability of the proposed device for detecting tumors during VATS, solid lesions located deep in the lung parenchyma were resected and X-ray images were obtained. Because our device has not yet been approved as a medical device, in this preliminary experiment, the lung lesions were scanned after resection.

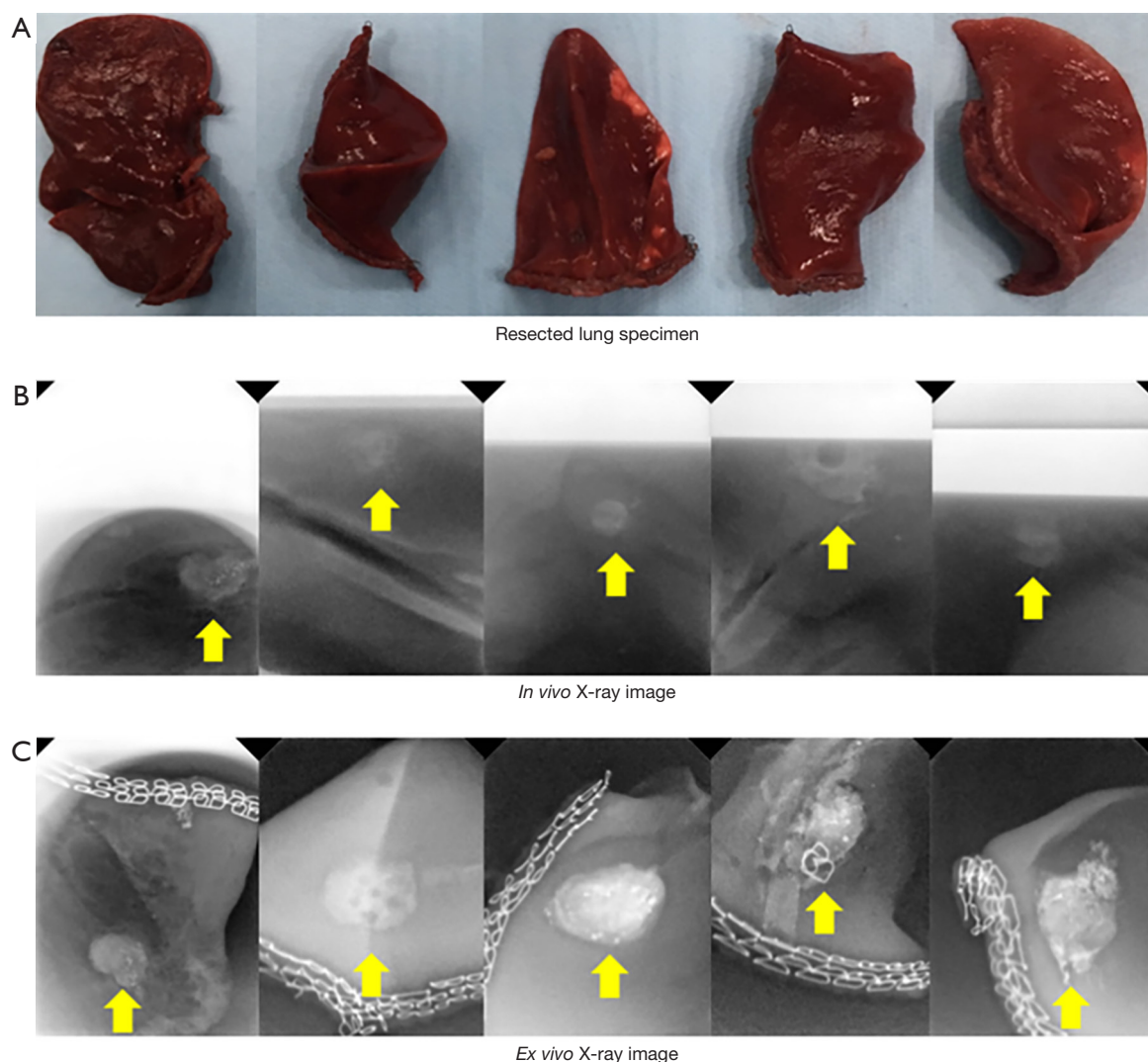


**Figure 3** *In vivo* and *ex vivo* X-ray images of pseudolesions in the lung samples of pigs. (A) Resected lung tissues; (B) *in vivo* images; (C) *ex vivo* images.

In three patients with lung cancer, anatomical resection was performed using a VATS technique, and the specimen was removed. The lesions were then palpated and marked using a needle. In the X-ray images obtained using the proposed device, a solid lesion appeared in the right lower lobe. No radiocontrast or hook wire was inserted before VATS. This case demonstrates that our method can clearly visualize solid tumors in the lung parenchyma without the need to insert preoperative radiocontrast agents (*Figure 4*).

In non-solid lesions of lung specimens, localization might be needed to identify the resection line for accurate resection as the target is not visible and not palpable (*Figure 5*). The images from our proposed device (*Figure 5D*) clearly

showed a localized lesion with radiocontrast compared with the images from C-arm fluoroscopy (*Figure 5E*).

## Discussion

In this study, we developed an ultra-low-dose *in situ* X-ray imaging device that supports VATS in real time. In animal studies, we demonstrated that our device provided X-ray images of the localized lung nodules with a sufficiently high spatial resolution and remarkably reduced radiation exposure to the surgical team. It was also possible to detect solid lesions in lung cancer specimens from patients using the proposed device even without the use of radiocontrast.

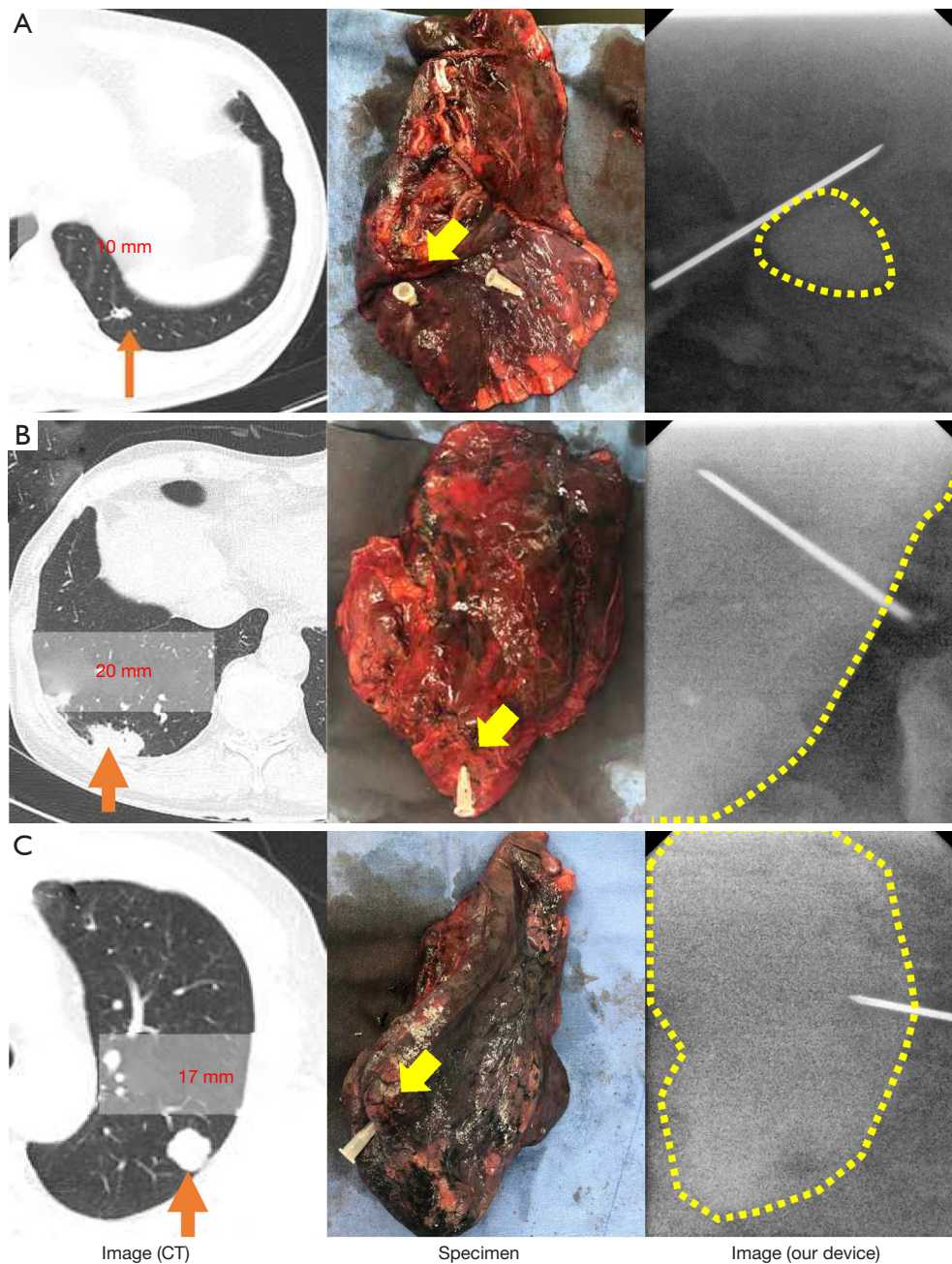


**Figure 4** X-ray image of human lung cancer specimens acquired using computed tomography (CT) and our device without injecting radiocontrast agent. (A) Case of a 55-year-old male patient with a 10-mm-sized solid lesion in the left lower lobe of the lung with suspected lung metastasis from colorectal cancer. (B) Case of a 68-year-old male patient with 20-mm-sized primary early lung cancer in the right lower lobe. (C) Case of a 68-year-old male patient with 17-mm-sized primary lung cancer in the left upper lobe. Although no radiopaque contrast agents such as lipiodol were injected before or during the surgery, the X-ray images obtained using the proposed device clearly show the needle-marked solid lesion.

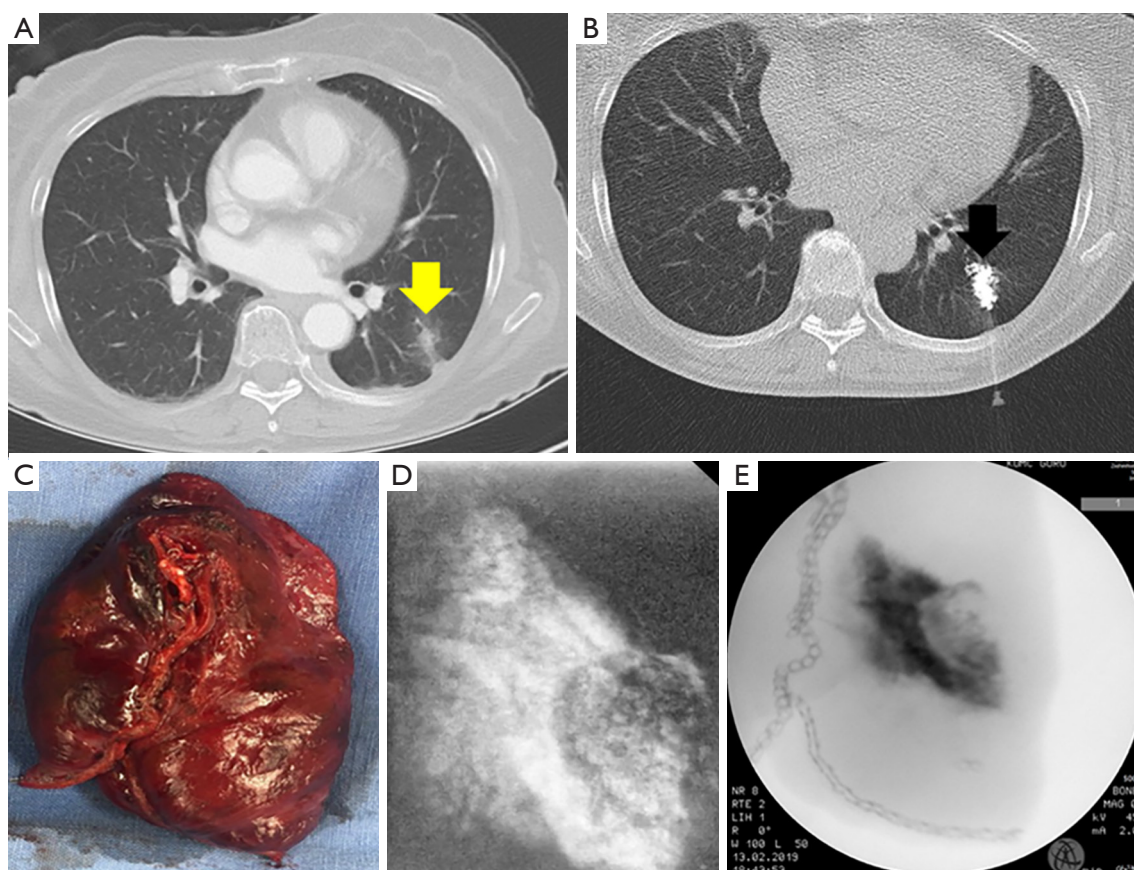


**Figure 5** Comparison of intraoperative image taken by our proposed device and C-arm fluoroscopic image in lung cancer specimen localized with radiocontrast. (A) Chest computed tomography (CT) scan of ground glass lesion (yellow arrow); (B) CT-guided injection of radiocontrast to the lung lesion (black arrow); (C) resected lung cancer specimen; (D) image taken by our device; and (E) fluoroscopic image of the lung cancer specimen.

These results indicate that the proposed method may be useful for identifying the pleural location at which the resection should begin. In addition, this feature allows us to obtain sufficient resection margins for sublobar resection of cancer, which is essential for reducing locoregional cancer recurrence (33,34).

The X-ray device proposed in this study yielded a significant reduction in radiation exposure. The radiation dose of our device was 53–130 nGy, which is only 1/400 of that used with C-arm fluoroscopy. The main reason for the reduced radiation dose and negligible temperature problem using the proposed device is that the distance between the X-ray source and sensor is small and the total thickness of the imaging subject is remarkably low. As the lesion and other organs do not overlap, the amount and penetration power of X-ray photons need not be as high as those of

C-arm fluoroscopy and CT (35,36). In addition, high-contrast X-ray images can be obtained because the ratio of the scattered X-ray photons is relatively small. We expect that further technical improvements to the device will be useful for finding small non-calcified pulmonary nodules that are difficult to be detected using C-arm technology. Meanwhile, a fluorescence based imaging technique is also widely used to further reduce radiation exposure during nodule localization. However, this technique still suffers from detecting the exact location owing to the spread of the fluorescent materials, or identifying deep-lying lesions. Moreover, the CT-based prelocalization procedure cannot be skipped as well.

Using the device proposed in this study, an image of a pulmonary nodule of interest can be acquired within 5 s, providing information on the resection margin of

the pulmonary nodule in near real-time. Because the approximate margin of resection can be identified through CT images obtained for diagnostic purposes before surgery, gross inspection of lung tissues using C-arm or cone beam CT in the operating room is currently quite redundant.

Moreover, rapid acquisition time and temperature stability allow repetitive scanning with our device, preventing the transition to open surgery, which can be caused by incorrect resection or improper removal of the nodule-of-interest (37).

Our proposed device is worth considering for image-guided surgery using robots. However, as there is no tactile sensation during robotic surgery, palpation of nodules is limited in sublobar resection of lung lesions (38). It is also difficult to use C-arm or cone-beam CT in an operating room equipped with a robotic system. Therefore, combining our new real-time intraoperative imaging device with a robotic device will be useful for localizing lesions and determining surgical margins during robotic surgery. Potentially, our device also might provide a feasible method in laparoscopic gastrointestinal surgery with endoscopic marking to achieve safe resection margin with or without fluorescent dye (39).

### Limitation

Our device showed the limitation in detecting non-solid lesions without the use of a radiologic marker. The detection of non-solid lesions, such as ground glass opacity (GGO) lesions, is still challenging even in open surgery with finger palpation. We are currently improving our X-ray device by utilizing an advanced CNT X-ray source (i.e., small but with high X-ray output) and high-resolution digital image sensor. We believe that our next-generation X-ray device would potentially be beneficial in detecting the GGO lesions without using radiologic markers along with the help of an artificial intelligence-based image analysis technology.

To use the proposed X-ray device in clinical practice, an additional research and development to reduce the device size is needed. Currently, in VATS, the size of the incision for the camera and devices is 5–20 mm, or in the case of a wound protector, it has an oval shape of 30–40 mm. The CNT-based source we currently use has a diameter of 15 mm; however, after adding electrical and radiation shields, the diameter increases to 46 mm. Currently, research is underway to minimize the size of the final device by reducing the diameter of the CNT source to 7 mm and lowering the tube

voltage required for X-ray imaging. For intrathoracic use, the diameter of the devices should be 20–30 mm. A circular stapler with a diameter of 28–33 mm is used through the narrow intercostal space during thoracoscopic esophageal cancer surgery, which is expected to be the largest diameter of the instrument that can be used without significant interference (40,41).

Careful consideration of radiation and electrical safety is necessary because our devices are used in the body and can directly affect internal organs. There are devices that irradiate X-rays for therapeutic purposes by placing them in a body cavity, and our device is relatively safe because it requires significantly lower X-ray tube voltages and currents than those required for treatment purposes (42). Further investigations on the user convenience of the proposed device based on the requests of thoracic surgeons are also required.

### Conclusions

In this study, we introduced a novel concept of an intraoperative X-ray imaging device that can be useful for VATS and demonstrated its feasibility by performing *in vivo* and *ex vivo* studies of pseudonodules using animal models and preliminarily acquiring X-ray images of human lung nodules without injecting radiocontrast agents.

### Acknowledgments

We thank LIVSMED, VSI, and HDX for supporting the mechanical design and providing the X-ray sources and sensors. We also thank the veterinary team at the Korea University Medical Center (KUMC) for supporting animal experiments.

*Funding:* This work was supported by grants from the Korea Evaluation Institute of Industrial Technology funded by the Korean Ministry of Trade, Industry and Energy (Grant No. 2015-4-10052467) and the Korea Medical Device Development Fund grant funded by the Korean government (the Ministry of Science and ICT, Ministry of Trade, Industry and Energy, Ministry of Health & Welfare, Ministry of Food and Drug Safety) (Project No. 1711138151, KMDF\_PR\_20200901\_0094\_02).

### Footnote

*Reporting Checklist:* The authors have completed the ARRIVE reporting checklist. Available at <https://tclr>.

[amegrouops.com/article/view/10.21037/tlcr-21-909/rc](https://amegrouops.com/article/view/10.21037/tlcr-21-909/rc)

*Data Sharing Statement:* Available at <https://tlcr.amegrouops.com/article/view/10.21037/tlcr-21-909/dss>

*Peer Review File:* Available at <https://tlcr.amegrouops.com/article/view/10.21037/tlcr-21-909/prf>

*Conflicts of Interest:* All authors have completed the ICMJE uniform disclosure form (available at <https://tlcr.amegrouops.com/article/view/10.21037/tlcr-21-909/coif>). The authors have no conflicts of interest to declare.

*Ethical Statement:* The authors are accountable for all aspects of the work in ensuring that questions related to the accuracy or integrity of any part of the work are appropriately investigated and resolved. Animal experiments were performed under a project license (No. KOREA-2017-0030) granted by institutional review board of Korea University College of Medicine, in compliance with institutional guidelines for the care and use of animals. The study was conducted in accordance with the Declaration of Helsinki (as revised in 2013) and approved by institutional board of Korea University Guro Hospital (No. 2017GR0018). Informed consent has been obtained from all individual participants included in this study.

*Open Access Statement:* This is an Open Access article distributed in accordance with the Creative Commons Attribution-NonCommercial-NoDerivs 4.0 International License (CC BY-NC-ND 4.0), which permits the non-commercial replication and distribution of the article with the strict proviso that no changes or edits are made and the original work is properly cited (including links to both the formal publication through the relevant DOI and the license). See: <https://creativecommons.org/licenses/by-nc-nd/4.0/>.

## References

1. Siegel RL, Miller KD, Jemal A. Cancer statistics, 2019. *CA Cancer J Clin* 2019;69:7-34.
2. DeSantis CE, Miller KD, Dale W, et al. Cancer statistics for adults aged 85 years and older, 2019. *CA Cancer J Clin* 2019;69:452-67.
3. Brownlee AR, Donington JS. Update on Lung Cancer Screening. *Semin Respir Crit Care Med* 2020;41:447-52.
4. Choi JW, Park CM, Goo JM, et al. C-arm cone-beam CT-guided percutaneous transthoracic needle biopsy of small ( $\leq 20$  mm) lung nodules: diagnostic accuracy and complications in 161 patients. *AJR Am J Roentgenol* 2012;199:W322-30.
5. Tam AL, Kim ES, Lee JJ, et al. Feasibility of image-guided transthoracic core-needle biopsy in the BATTLE lung trial. *J Thorac Oncol* 2013;8:436-42.
6. Rivera MP, Mehta AC, Wahidi MM. Establishing the diagnosis of lung cancer: Diagnosis and management of lung cancer, 3rd ed: American College of Chest Physicians evidence-based clinical practice guidelines. *Chest* 2013;143:e142S-65S.
7. Winckelmans T, Decaluwé H, De Leyn P, et al. Segmentectomy or lobectomy for early-stage non-small-cell lung cancer: a systematic review and meta-analysis. *Eur J Cardiothorac Surg* 2020;57:1051-60.
8. El-Sherif A, Gooding WE, Santos R, et al. Outcomes of sublobar resection versus lobectomy for stage I non-small cell lung cancer: a 13-year analysis. *Ann Thorac Surg* 2006;82:408-15; discussion 415-6.
9. Kodama K, Doi O, Higashiyama M, et al. Intentional limited resection for selected patients with T1 N0 M0 non-small-cell lung cancer: a single-institution study. *J Thorac Cardiovasc Surg* 1997;114:347-53.
10. Kodama K, Higashiyama M, Okami J, et al. Oncologic Outcomes of Segmentectomy Versus Lobectomy for Clinical T1a N0 M0 Non-Small Cell Lung Cancer. *Ann Thorac Surg* 2016;101:504-11.
11. McDermott S, Fintelmann FJ, Bierhals AJ, et al. Image-guided Preoperative Localization of Pulmonary Nodules for Video-assisted and Robotically Assisted Surgery. *Radiographics* 2019;39:1264-79.
12. Park CH, Han K, Hur J, et al. Comparative Effectiveness and Safety of Preoperative Lung Localization for Pulmonary Nodules: A Systematic Review and Meta-analysis. *Chest* 2017;151:316-28.
13. Doo KW, Yong HS, Kim HK, et al. Needleoscopic resection of small and superficial pulmonary nodule after computed tomographic fluoroscopy-guided dual localization with radiotracer and hookwire. *Ann Surg Oncol* 2015;22:331-7.
14. Gossot D, Miaux Y, Guermazi A, et al. The hook-wire technique for localization of pulmonary nodules during thoracoscopic resection. *Chest* 1994;105:1467-9.
15. Klinkenberg TJ, Dinjens L, Wolf RFE, et al. CT-guided percutaneous hookwire localization increases the efficacy and safety of VATS for pulmonary nodules. *J Surg Oncol* 2017;115:898-904.
16. Park CH, Lee SM, Lee JW, et al. Hook-wire localization

- versus lipiodol localization for patients with pulmonary lesions having ground-glass opacity. *J Thorac Cardiovasc Surg* 2020;159:1571-1579.e2.
17. Finley RJ, Mayo JR, Grant K, et al. Preoperative computed tomography-guided microcoil localization of small peripheral pulmonary nodules: a prospective randomized controlled trial. *J Thorac Cardiovasc Surg* 2015;149:26-31.
  18. Lempel JK, Raymond DP. Intraoperative Percutaneous Microcoil Localization of Small Peripheral Pulmonary Nodules Using Cone-Beam CT in a Hybrid Operating Room. *AJR Am J Roentgenol* 2019;213:778-81.
  19. Hasegawa T, Kuroda H, Sato Y, et al. The Utility of Indigo Carmine and Lipiodol Mixture for Preoperative Pulmonary Nodule Localization before Video-Assisted Thoracic Surgery. *J Vasc Interv Radiol* 2019;30:446-52.
  20. Kang DY, Kim HK, Kim YK, et al. Needle-scopy-assisted resection of pulmonary nodule after dual localisation. *Eur Respir J* 2011;37:13-7.
  21. Kim YD, Jeong YJ, I H, et al. Localization of pulmonary nodules with lipiodol prior to thoracoscopic surgery. *Acta Radiol* 2011;52:64-9.
  22. Liu Z, Yang R, Shao F, et al. Localization of Small Peripheral Pulmonary Lesion by Methylene Blue Injection With Radial Endobronchial Ultrasonography in Sublobar Resection. *Ann Thorac Surg* 2016;101:e57-9.
  23. Rho J, Lee JW, Quan YH, et al. Fluorescent and Iodized Emulsion for Preoperative Localization of Pulmonary Nodules. *Ann Surg* 2021;273:989-96.
  24. Han KN, Kim HK. The feasibility of electromagnetic navigational bronchoscopic localization with fluorescence and radiocontrast dyes for video-assisted thoracoscopic surgery resection. *J Thorac Dis* 2018;10:S739-48.
  25. Nomori H, Horio H, Naruke T, et al. Fluoroscopy-assisted thoracoscopic resection of lung nodules marked with lipiodol. *Ann Thorac Surg* 2002;74:170-3.
  26. Toba H, Kondo K, Miyoshi T, et al. Fluoroscopy-assisted thoracoscopic resection after computed tomography-guided bronchoscopic metallic coil marking for small peripheral pulmonary lesions. *Eur J Cardiothorac Surg* 2013;44:e126-32.
  27. Anayama T, Hirohashi K, Okada H, et al. Simultaneous cone beam computed tomography-guided bronchoscopic marking and video-assisted thoracoscopic wedge resection in a hybrid operating room. *Thorac Cancer* 2019;10:579-82.
  28. Rouzé S, de Latour B, Flécher E, et al. Small pulmonary nodule localization with cone beam computed tomography during video-assisted thoracic surgery: a feasibility study. *Interact Cardiovasc Thorac Surg* 2016;22:705-11.
  29. Kawakita N, Takizawa H, Kondo K, et al. Indocyanine Green Fluorescence Navigation Thoracoscopic Metastasectomy for Pulmonary Metastasis of Hepatocellular Carcinoma. *Ann Thorac Cardiovasc Surg* 2016;22:367-9.
  30. Yamashita S, Tokuishi K, Anami K, et al. Video-assisted thoracoscopic indocyanine green fluorescence imaging system shows sentinel lymph nodes in non-small-cell lung cancer. *J Thorac Cardiovasc Surg* 2011;141:141-4.
  31. Meisinger QC, Stahl CM, Andre MP, et al. Radiation Protection for the Fluoroscopy Operator and Staff. *AJR Am J Roentgenol* 2016;207:745-54.
  32. Gilula LA, Barbier J, Totty WG, et al. Radiation shielding device for fluoroscopy. *Radiology* 1983;147:882-3.
  33. El-Sherif A, Fernando HC, Santos R, et al. Margin and local recurrence after sublobar resection of non-small cell lung cancer. *Ann Surg Oncol* 2007;14:2400-5.
  34. Moon Y, Park JK, Lee KY. The Effect of Resection Margin Distance and Invasive Component Size on Recurrence After Sublobar Resection in Patients With Small ( $\leq 2$  Cm) Lung Adenocarcinoma. *World J Surg* 2020;44:990-7.
  35. Kubo T, Lin PJ, Stiller W, et al. Radiation dose reduction in chest CT: a review. *AJR Am J Roentgenol* 2008;190:335-43.
  36. Lin EC. Radiation risk from medical imaging. *Mayo Clin Proc* 2010;85:1142-6; quiz 1146.
  37. Nakashima S, Watanabe A, Obama T, et al. Need for preoperative computed tomography-guided localization in video-assisted thoracoscopic surgery pulmonary resections of metastatic pulmonary nodules. *Ann Thorac Surg* 2010;89:212-8.
  38. Ramadan OI, Wei B, Cerfolio RJ. Robotic surgery for lung resections-total port approach: advantages and disadvantages. *J Vis Surg* 2017;3:22.
  39. Dickler A, Ivanov O, Francescatti D. Intraoperative radiation therapy in the treatment of early-stage breast cancer utilizing soft axent electronic brachytherapy. *World J Surg Oncol* 2009;7:24.
  40. Nguyen TN, Hinojosa MW, Smith BR, et al. Thoracoscopic construction of an intrathoracic esophagogastric anastomosis using a circular stapler: transoral placement of the anvil. *Ann Thorac Surg* 2008;86:989-92.
  41. Caso R, Wee JO. Esophagogastric Anastomotic

Techniques for Minimally Invasive and Robotic Ivor Lewis Operations. *Operative Techniques in Thoracic and Cardiovascular Surgery* 2020;25:105-23.

42. Eaton DJ. Electronic brachytherapy--current status and future directions. *Br J Radiol* 2015;88:20150002.

**Cite this article as:** Park H, Han KN, Choi BH, Yoon H, An HJ, Lee JS, Kim HK. Ultra-low-dose intraoperative X-ray imager for minimally invasive surgery: a pilot imaging study. *Transl Lung Cancer Res* 2022;11(4):588-599. doi: 10.21037/tlcr-21-909

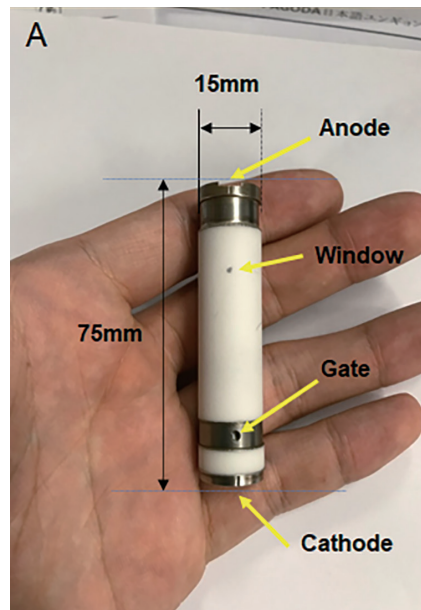


**Figure S1** Carbon nanotube (CNT)-based X-ray source. The CNT X-ray source features a tri-polar structure comprising Anode, Cathode, and Gate. All the X-ray irradiations can be digitally controlled with high speed and high precision. Also, the CNT-based compact X-ray source can significantly reduce size and weight of the X-ray imaging device because the X-ray emission is performed via quantum tunneling of electrons without requiring any heating materials, such as filaments. Therefore, the CNT-based X-ray source is suitable option for developing intraoperative X-ray imager without causing any heat or power consumption issues during minimally invasive surgery.

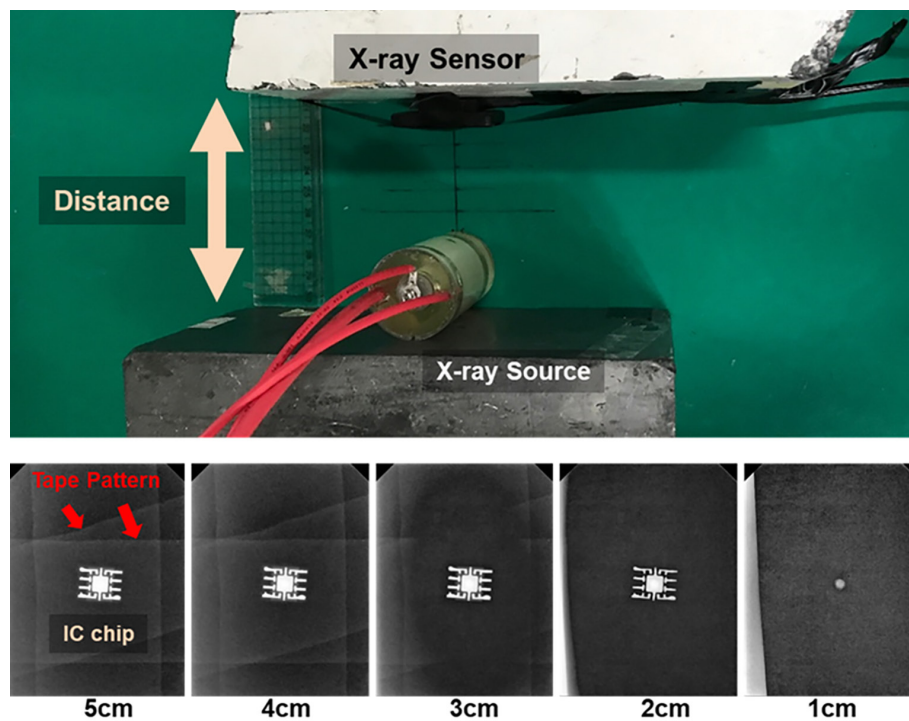


**Figure S2** Experiment to determine the optimal distance between X-ray source and sensor. (A) Experimental setup; (B) X-ray images of an IC chip with different source-to-sensor distances (tube voltage =40 kVp, tube current =2 mA, exposure time =20 ms).

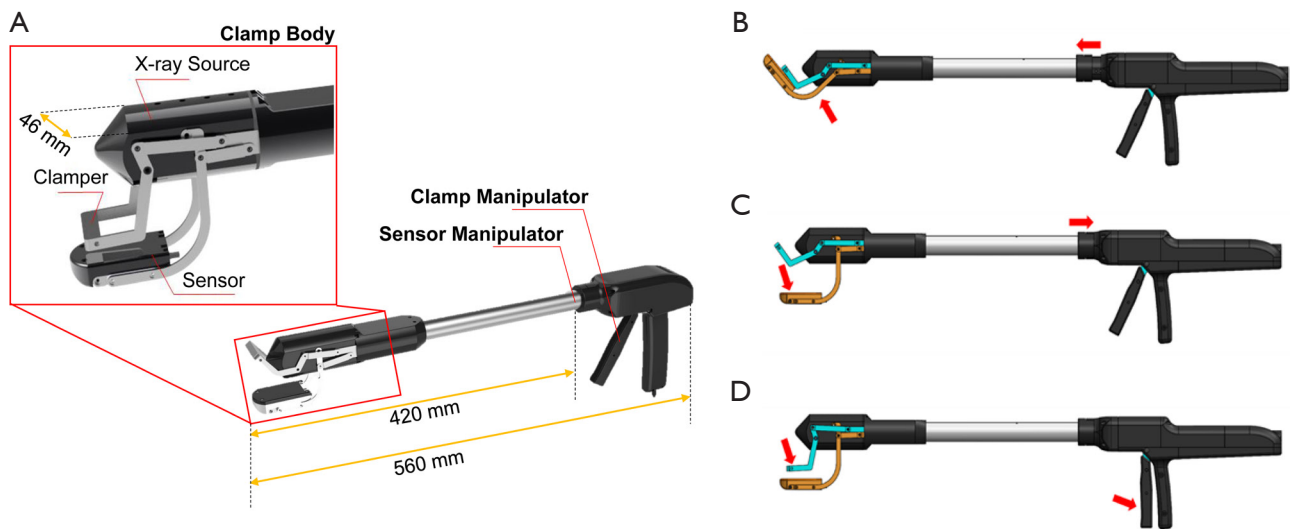


**Figure S3** Drawing and operation protocol of the proposed intraoperative X-ray imager. (A) Drawing of the proposed device consisting of a clamp body, sensor manipulator, and clamp manipulator. Step-by-step operation protocol of the proposed device: (B) Insert mode, (C) Ready mode, and (D) Clamp mode.

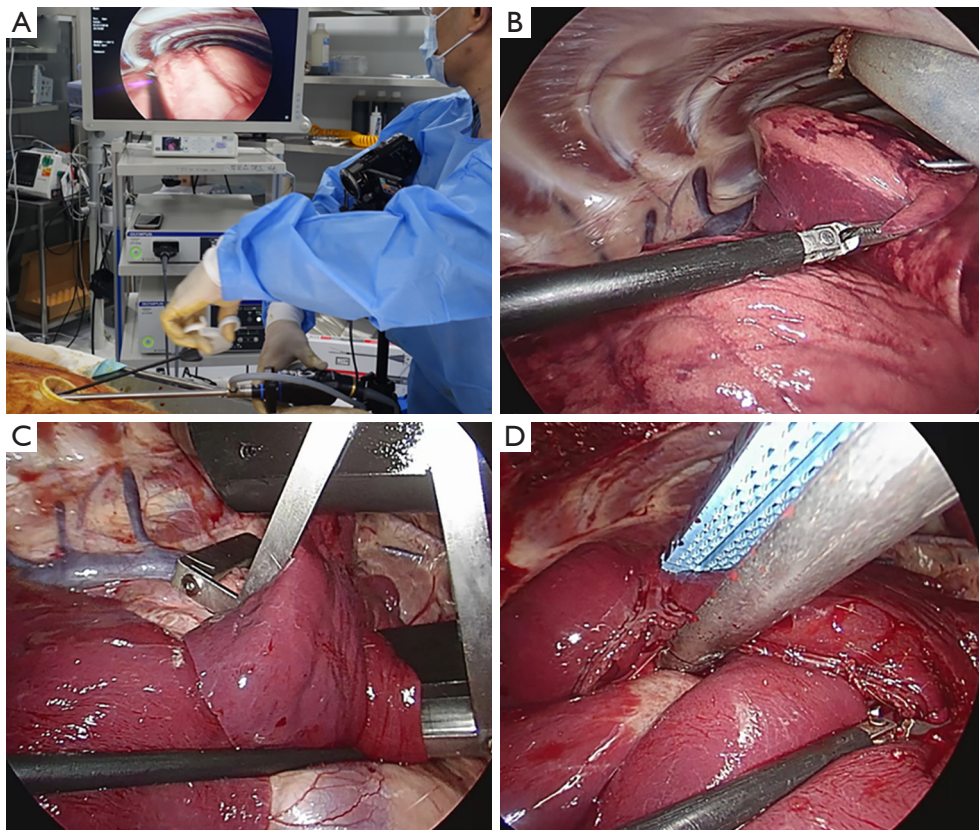


**Figure S4** Minimally invasive thoracoscopic surgery in a dog to investigate the feasibility of the proposed X-ray imager. (A) Dog surgery; (B) localization with agar and Lipiodol; (C) detection of lung nodule with the X-ray device; (D) resection of the lesion by stapling.

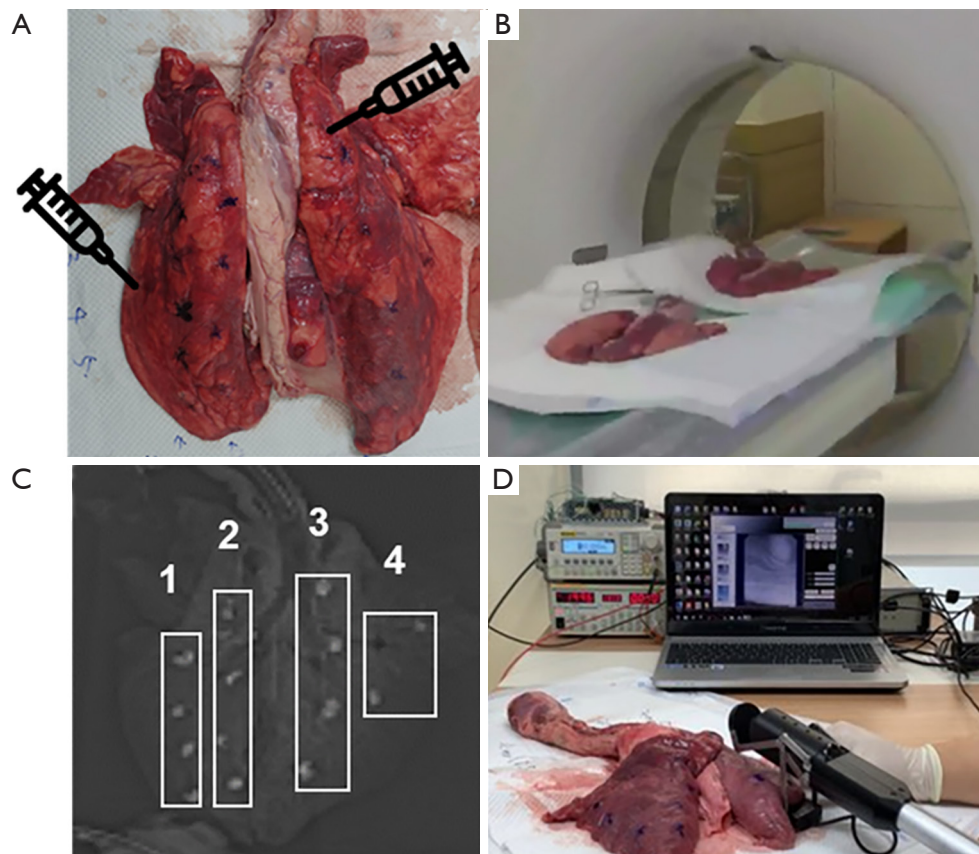


**Figure S5** Lesion detectability assessment depending on the concentration of contrast agent and the depth of the lesion. (A) *Ex vivo* specimen of porcine lung tissue with pseudo lung nodules. (B) CT scanning. (C) Scout X-ray image of the lung acquired using the CT machine. The numbers above the boxes correspond to the groups summarized in *Table 1*. (D) Pseudo lung lesion scan using the proposed device.

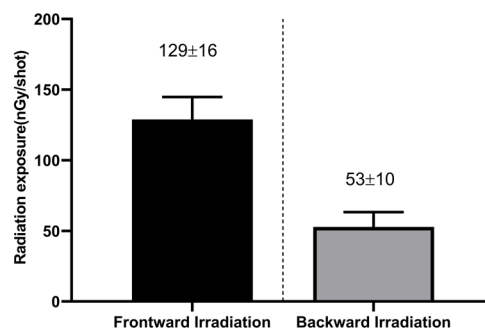


**Figure S6** Equivalent radiation dose measured using a calibrated radiation dosimeter. The dosimeter was installed 1 m away from the X-ray focal spot, and the radiation dose was measured and averaged over 10 consecutive X-ray shots.

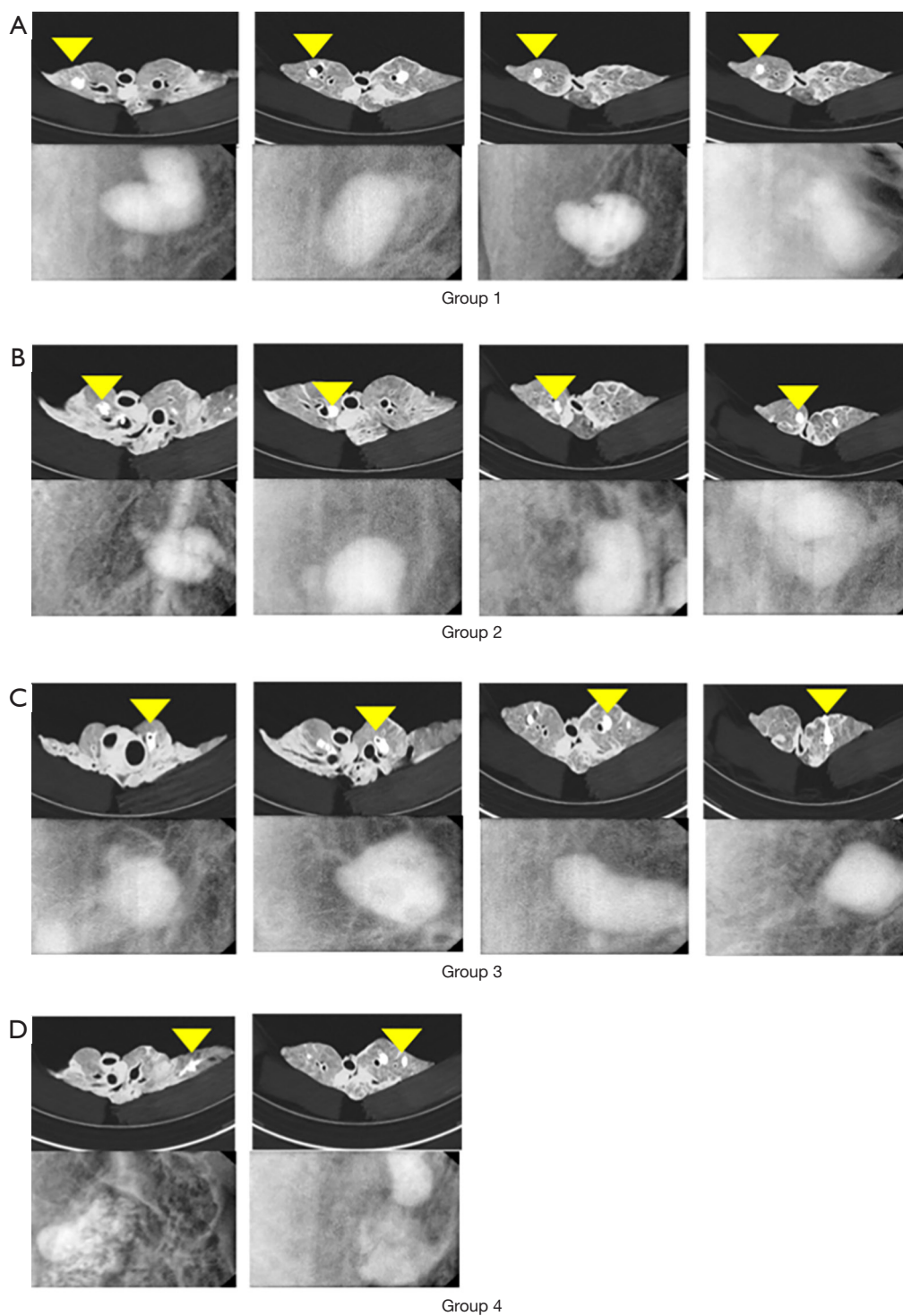


**Figure S7** Comparison of X-ray images obtained using CT machine (up) and the proposed device (down). Pseudo lung lesions in pigs were created with different volumes of an agar/Lipiodol mixture and in different pleural depths. (A) Group 1: 1 mL and 0.5 cm. (B) Group 2: 2 mL and 0.5 cm. (C) Group 3: 1 mL and 1 cm. (D) Group 4: 2 mL and 1 cm.

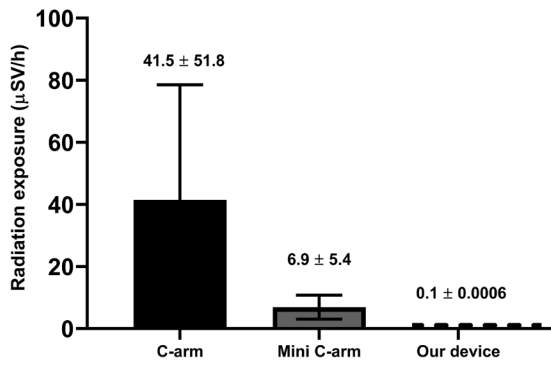


**Figure S8** Radiation exposure during intraoperative real-time X-ray imaging for pseudo lung lesion detection with radiocontrast agent. Our device ( $0.1 \pm 0.0006 \mu\text{Sv/h}$ ) yielded the lowest radiation exposure as compared to the conventional C-arm fluoroscopy ( $41.5 \pm 51.8 \mu\text{Sv/h}$ ) and mini C-arm used for dental or hand surgery ( $6.9 \pm 5.4 \mu\text{Sv/h}$ ).

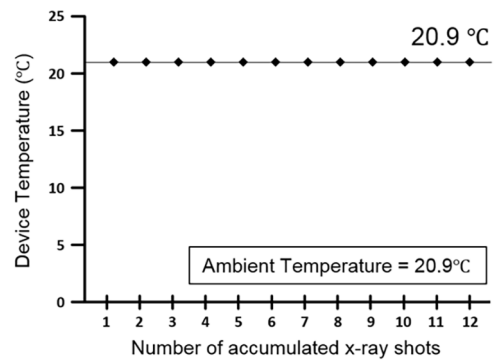


**Figure S9** Temperature measurements of the proposed device while performing 12 consecutive X-ray irradiations every 5 s. The parameters for X-ray irradiation were identical to those for other imaging experiments with a tube voltage of 40 kVp, a tube current of 2 mA, and an exposure time of 20 ms.

**Table S1** SNR values of detected pseudo lung lesions in the X-ray image

	Group 1	Group 2	Group 3	Group 4
1st row	14.39	16.22	18.28	19.28
2nd row	17.70	17.96	15.27	17.32
3rd row	17.34	19.95	14.52	N/A
4th row	14.51	17.04	14.90	N/A

SNR, signal-to-noise ratio (unit: dB); N/A, not applicable.